

Synthesis and Characterization of Ag-Modified Composites as Counter Electrodes for Solar Cell Applications

Ramkumar Singh Dandolia^{1,*}, Arvind Dandotia¹, S.S. Tomar², Radha Tomar³

¹School of studies in Physics, Jiwaji University, Gwalior-474011, India

²Govt. S.L.P.P.G. College, Morar- Gwalior-474006, India

³School of studies in Chemistry, Jiwaji University, Gwalior-474011, India

*Corresponding author:

Ramkumar Singh Dandolia

School of studies in Physics, Jiwaji University,
Gwalior-474011, India,
E-mail: r.k.dandolia@gmail.com

Received : September 02, 2024

Published : January 06, 2025

ABSTRACT

Crystalline zeolite nanoparticles are successfully synthesized via the hydrothermal method and this zeolite was modified by using the ion exchange method. Polypyrrole/Zeolite nanocomposite was done by using polymerization techniques. The synthesized samples were characterized via different techniques like X-Ray Powder diffraction (XRD), Fourier Transformation Infra-Red Spectroscopy (FTIR), and Scanning electron microscopy (SEM) with EDAX, The XRD pattern confirms the hexagonal phase of the synthesized zeolite material. The composite material is crystalline in nature, with an average crystallite size of 35 nm. The SEM micrograph displays a regular hexagonal rod shape. Although, a dramatic shift is observed in the band gap of the samples is usually reduced up to 1.74 eV from 2.58 eV. The concentrations of the binder added to the composite pastes were varied to investigate their effect on the physical properties of the counter electrode and the electronic properties of the constructed DSSC.

Keywords: Zeolite, Nanoparticle, Synthesis, Photocatalysis, Spectroscopy.

INTRODUCTION

From the last few centuries, the field of Zeolite opens a new ray for researchers in order to explore the scientific community and engineering technology. Zeolites are one of the most commonly used solid catalysts in the material science and chemical industry because of their unique microporous frameworks and shape selectivity [1,2]. Several zeolites are used for the performance of catalysis but the Zeolite-Linde Type L (LTL) is better option for photocatalysis. Earlier reports investigated that Zeolite-Linde Type L have 1D-12 membered ring channels [3,4]. In addition to that these zeolites possess some important properties which shows the requirement for better scientific advancement. The Zeolite-Linde Type L shows best properties especially for the longer chains,

due to the diffusion limitation of one-dimensionally linear channels [5,6]. During the past few years, synthesis and catalytic applications of nano-sized zeolites with shorter channels have been proven to be an effective strategy for enhancing the performance in a variety of diffusion-limited hydrocarbon conversions [7,8]. Due to waste consumption and contamination, the growth of industries poses a serious threat to the environment worldwide. More efforts should be made to reduce environment pollution. One effective method to address this significant issue is by photocatalysis [9]. Although numerous types of materials are employed for catalysis such as chalcogenides, metal oxides and perovskites [10,11]. Zeolites' porous cage like structure finds numerous applications, including gas detection and cleaning [12,13]. Zeolites can be successfully synthesized by several methods, such as the salinization, confined space synthesis and microwave synthesis method [14,15]. Nano-sized Zeolite-Linde Type L prepared by microwave method had been reported. Due to the less stability of these metal oxides and perovskites, researchers have found that Zeolites are considered to be the prime candidate for photocatalysis because of high selectivity to C-8 aromatics in n-octane aromatization due to the lower extent of secondary hydrogenolysis [16]. However, the microwave synthesis method is considering as energy consuming and not suitable for industrial applications and technological catalysis [17]. Therefore, it is extremely desirable to develop a cost-effective and easy scale-up approach to prepare nano-sized Linde Type L Zeolites with improved catalytic performance. Fortunately, a few researchers have observed that the incorporation of a small quantity of barium could facilitate the formation of nano-sized Linde Type L Zeolites [18]. To the best of our knowledge, the explanation for the effect of Ba on the Linde Type L crystallization process is still unclear. The comprehensive understanding of the formation process is also significant for more scientifically modulating Zeolite crystal sizes. In addition to that the systematic study for the effect of Linde Type L crystal sizes on the n-alkane aromatization needs to be further addressed. Non-acidic Linde Type L Zeolite of one-dimensional 12-membered ring channels of 0.71 nm with platinum loading exhibits the exceptional performance of alkane aromatization as first reported by Bernard et al. Nano-sized Linde Type L Zeolite was successfully synthesized via the hydrothermal method [19,20]. Zeolite-Linde Type L has a hexagonal crystal structure (space group P-6/mmm) with unit cell constants $a = b = 18.4$ and $c = 7.5$ [21,22]. Zeolite-Linde Type L has attracted a lot of attention in the last 20

years because of its uses in catalytic processes, separations, and photonic devices [23]. For many years, iron catalysts supported on various materials have been frequently used in Fischer-Tropsch processes. By combining the benefits of iron and Linde Type L Zeolites, ultra-fine Fe-Linde Type L Zeolite nanocrystals may be synthesized, which could be useful in catalytic and ion exchange applications. In this work, nano-sized Linde Type L Zeolites were successfully synthesized via the hydrothermal method. The synthesized material was characterized by various techniques including X-ray diffraction (XRD), ultraviolet-visible (UV-Vis) spectroscopy, scanning electron microscope (SEM), Fourier transforms infrared spectrometer (FT-IR), more importantly, and the synthesis sample used the check performance of photovoltaic activities analysis.

Experimental Section

Reagents

Potassium Hydroxide, Silica Sol, Aluminium Hydroxide, Magnesium Nitrate, Copper Nitrate, and Pyrrole is purchased from Fisher Scientific, sigma, CDH Company, Merck, Fisher Scientific, Sigma. The entire chemical used in the synthesis is analytical grade and does not need further purification.

Synthesis of Zeolite- Linde Type L

The synthesis of Zeolite-Linde Type L has been carried out by taking 10.13 g Potassium Hydroxide, 5.27 g Aluminium Hydroxide is dissolved in 16.66 ml double distilled water and the reaction mixture is heated until a clear solution 'A' is obtained. Solution A is allowed to cool to room temperature. In a separate beaker 50.08 ml silica sol, 4.83 g magnesium nitrate solution was added to 33.0 ml of de-ionized water and mixed by stirring for about 3 minutes until a homogeneous solution 'B' is formed. Then the solution A and B are mixed to form a homogeneous suspension and 8.33 ml of de-ionized water are added to it. The above suspension solution is stirred until thickening starts. The resulting gel is placed in a Teflon-lined autoclave and kept in an oven preheated to 175° C for 48 hours then after, the autoclave is removed from the oven and immersed in cool de-ionized water. The material inside the autoclave is centrifuged at 10,000 rpm and washed until its pH value reaches 9 and subsequently dried at 150°C in an oven for 16 h. The dried sample is crushed into a fine powder and calcined at 540°C for 7 hours.

Composite of Zeolite-LTL/PPy

1 gram of Zeolite-Linde Type L and 1 ml of Pyrrole are dispersed in 35 ml of de-ionized water and undergo sonication for 15 minutes. After sonication 0.72 Mole powder of $\text{FeCl}_3 \cdot 6\text{H}_2\text{O}$ is added to it and stirred it for 2 h. Finally, the composite is washed with double de-ionized water and dried at 50°C for 24 h in the oven.

Modified Zeolite to make a paste

To create a homogeneous paste with uniform composition, the required amount of Modified Zeolite powder was mixed with 15 ml of ethanol and stirred for 10 minutes; this solution is then placed in an ultra-sonicator for 15 minutes.

Fabrication of Devices cleaning of substrates

Fluorine-doped Tin Oxide (FTO) coated conducting glass substrates with a sheet resistance of $15\Omega/\text{cm}^2$ were cut into small pieces measuring $1 \times 1 \text{ cm}^2$ by using a diamond cutter. The substrates were then ultrasonically cleaned for 10 minutes each with detergent, ethanol, acetone, and de-ionized water. These cleaned substrates are dried in a hot air oven set to 60°C for 10 minutes. This type of cleaning ensures the removal of all dirt including dust, fingerprints, oil contents, and other contamination materials that were left behind after manufacture. This improves transparency while also providing a good conduction path for electron collection. Substrates should never be handled with the bare hands.

Deposition of nanocomposite paste on the substrates

A single-layer mask is produced on the conducting side for the photoanode using adhesive tape (Magic tape-cello type). The Mask is designed with a 0.25 cm^2 active. The required or desired amount of TiO_2 paste was applied to one edge of the unmasked area and uniformly spread over the substrate using the doctor blade technique.

Heat treatment for photoanode

The deposited paste-based film was left out untouched for 15 minutes. All Tapes were carefully removed and the film calcined at 450°C for 30 minutes and cooled to 80°C . In this

process, the film colour was brown at a higher temperature and turned to brownish-white when cooled down it. The calcination process was done to ensure the removal of all the solvents from the deposited layer on the film, leaving the tiny pores empty. It also promotes dye adsorption, which results in more excited electrons.

Dye sensitization of photoanode

The sensitization of a photoanode requires that the film be immersed in a dye solution for an extended period of time. Typically, this was accomplished by completely immersing photoanodes in the dye solution for 20-24 hours in a dark environment, after which the stray particles were washed off with ethanol to remove extra dye particles.

Preparation of the Counter Electrode

The CE preparation was done by cleaning FTO substrates as described in above section. Counter electrodes were prepared by a doctor blading technique, pasted of modified silver form Zeolite-polypyrrole paste onto the substrates, followed by calcination at 80°C for 15 minutes.

Assembling the dye-sensitized solar cell

The working electrode and CE were sandwiched together before applying thermoplastic sealant and pressing firmly against the hot plate at 100°C for 1 minute. The structure of the Solar cell is shown in figure 1 and the flow chart for the fabrication of this process is shown in figure 2.

Filling of Electrolytes

The high-stability electrolyte solvent was filled between the working and CEs then sealant by a paper clip. The final structure of the fabricated DSSC was connected to the crocodile clip with the multi-meter and checked the conductivity.

Characterization

The structural property of synthesis material is determined by the XRD studies using Rigaku Mini-flex 600 diffractometer at operating 40 kV and 30 mA in the 2θ Range 2° to 90° with

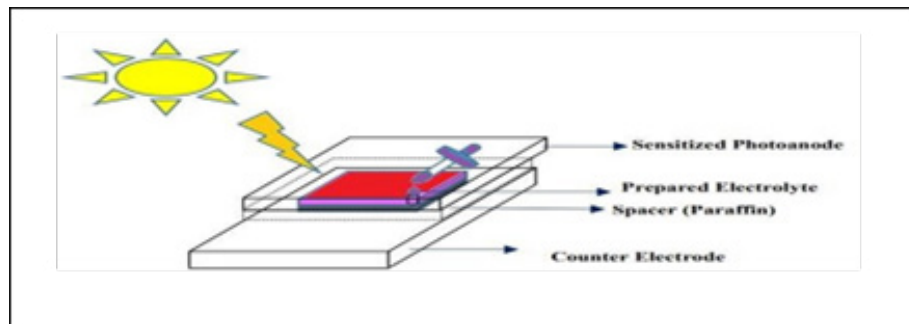


Figure 1. Fabrication of DSSC Solar cell.

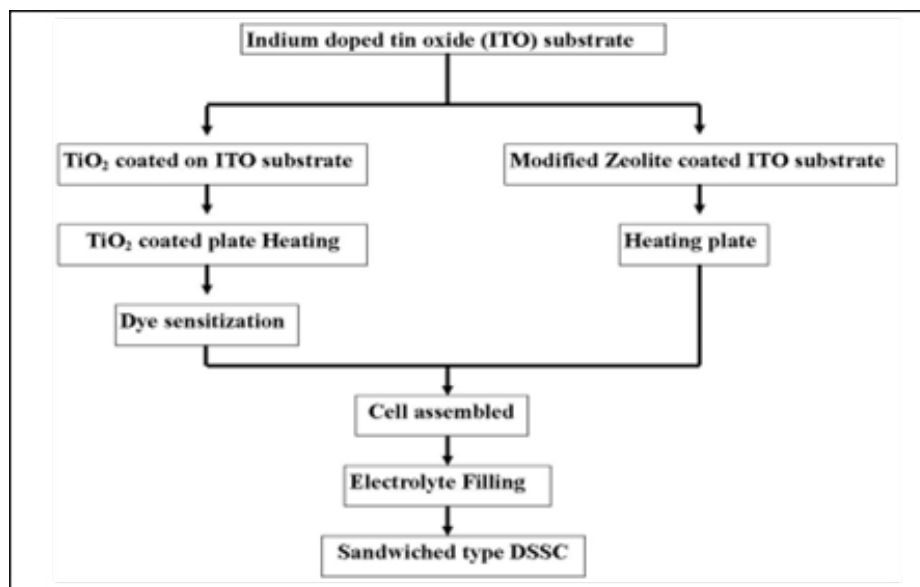


Figure 2. Flow chart of DSSC fabrication.

Cu K α (0.15406 Å) radiation. The analyses of SEM and Energy Dispersive Spectroscopy (EDS) were used to perform morphological and compositional analysis using Philips Model-Quanta 200 FEG. The FT-IR spectrum is recorded using a PerkinElmer spectrometer ranging from 450 to 4000 cm⁻¹.

RESULT AND DISCUSSION

XRD Analysis

The crystal structure, phase identification, crystallite size and presence of Zeolite Linde Type L (Zeolite-LTL), Polypyrrole (PPy) and Polypyrrole/Zeolite Linde Type L (PPy/Zeolite-LTL) nanoparticles samples were all analysed using Powder X-ray diffraction spectra. The diffraction peaks exemplify the presence of zeolite-Linde Type L and Polypyrrole thus verifying the formation of Polypyrrole/Zeolite-Linde Type L nanocomposites. The powder XRD patterns of zeolite-Linde Type L, Polypyrrole and Polypyrrole/Zeolite Linde Type

L nanoparticles are shown in Figure 3. All three samples have indicating different structures and showing different characteristic peaks. XRD patterns of both Zeolite Linde Type L and Polypyrrole samples showed sharp and distinct reflections indicate that the samples are highly crystalline. In both samples (Zeolite- Linde Type L and Zeolite- Linde Type L/Polypyrrole), the reflections are indexed based on the hexagonal crystal system which is showing good agreement with the Linde Type L Zeolite structure [25]. The ion exchange in the Zeolite with silver oxide and Polypyrrole does make a change in intensity only, not anything in Zeolite structural morphology. The crystallite size of Zeolite- Linde Type L is small when compared to Polypyrrole and Polypyrrole/zeolite- Linde Type L nano composite. This indicates that zeolite- Linde Type L offers a decreased crystallite size which thereby leads to a large surface area resulting in an increase in activity. Similarly, results were reported in the literature [26].

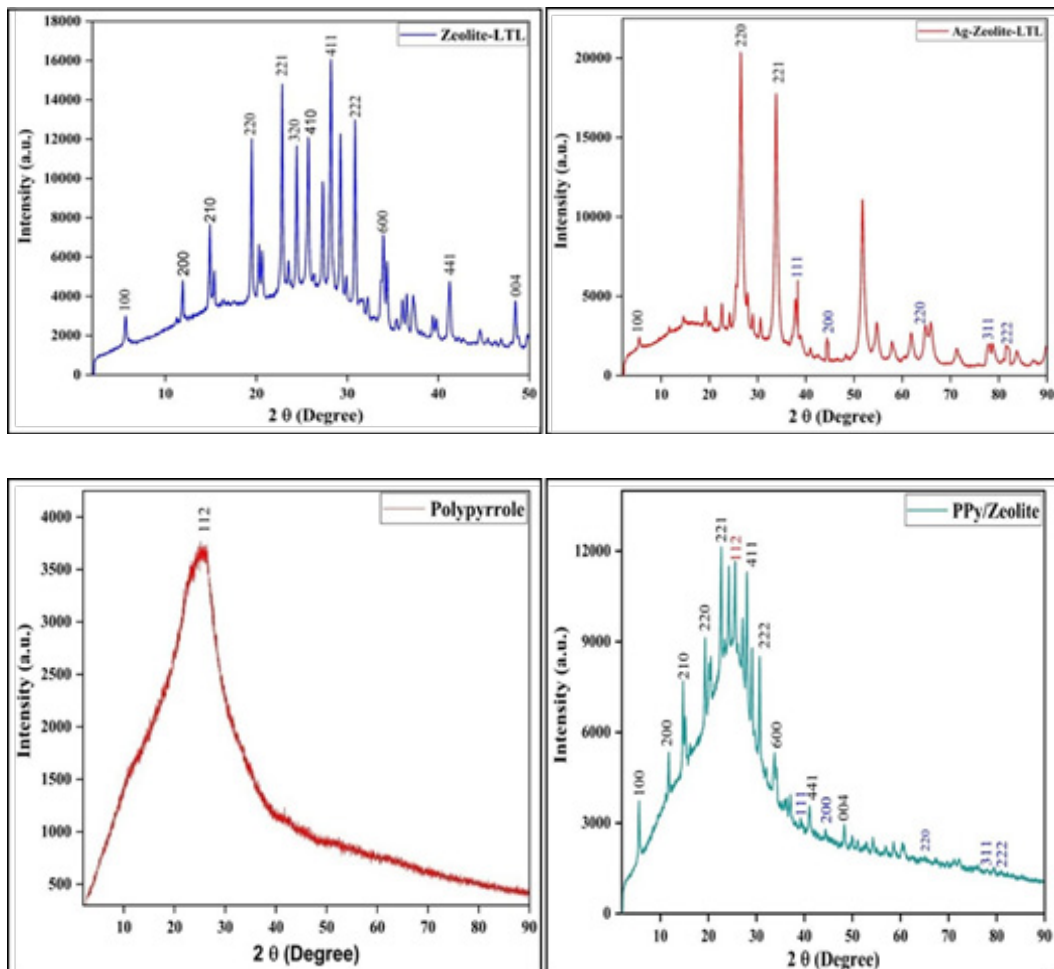


Figure 3. XRD Spectra of (a) Zeolite LTL, b) Ag-Zeolite-LTL, (c) PPy, (d) Composite

The average crystallite size of PPy/Zeolite-LTL nanocomposite was estimated by using Scherer's equation:

$$\beta = \frac{K\lambda}{L \cos\theta} \dots\dots\dots(1)$$

Where β is crystallite size in nm, K-crystal shape factor (have value 0.9 or 1.0), λ - wavelength Cu K α (1.542 Å), L-full width at half maxima (FWHM) and θ - is the Bragg's angle. The crystalline size of ion exchange Zeolite and composite are 35 nm and 33 nm respectively.

FT-IR Analysis

Fourier transforms infrared spectroscopy (FTIR) was used to identify the adsorption site and structure of the Zeolite samples. Figure 4 (a, b, c and d) shows the FTIR spectra of synthesized Zeolite and modified Zeolite. The FTIR graph shows the absorption band at around 461 cm⁻¹ and 613 cm⁻¹. The symmetric stretching bands were observed in 726 cm⁻¹ and 776 cm⁻¹. The asymmetric stretch vibration bands were

observed at 1027 cm⁻¹. Water binding molecules and OH stretching bands were found around 1643 cm⁻¹ and 3639 cm⁻¹ respectively [27,28]. The absorption peaks in Zeolite composite were obtained at (600, 666, 713, 853, 965, 1025, 1160, 1296, 1450, 1543, 1102, 2342, and 2659) cm⁻¹ which corresponding to the C-H bonding, the quinoid ring of vibration mode, C-N stretching of vibration, benzenoid ring stretching, the N-Quinoid ring stretching, N-H stretching vibrations respectively. All these peaks show the presence of Polypyrrole in the Zeolite composite [29].

SEM and Energy Dispersive X-ray (EDAX) Analysis

The morphology of the synthesized parent Zeolite and their composite-related images were more clearly observed by SEM.

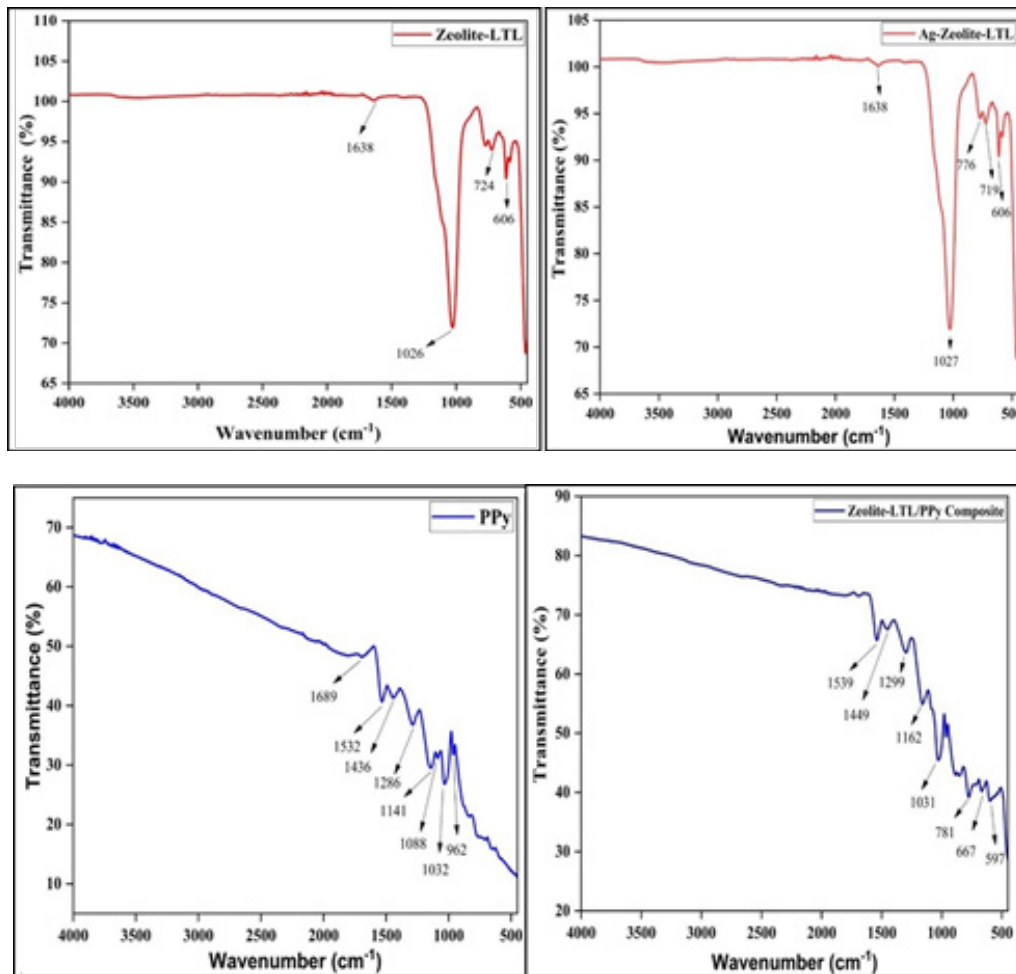


Figure 4. FTIR Spectra of (a) Zeolite LTL, (b) Ag-Zeolite-LTL, (c) PPy, (d) Composite.

The SEM images of synthesized material are shown in Figure 5 (a, b, c and d). These images show a regular hexagonal rod structure having an average length of 77.64 nm and a diameter of 23.52 nm. Due to the high surface charge, agglomeration and aggregation of crystals are visible and integrated [30,31]. The representation of the grains is regular and the microstructure consists of many neatly arranged rod-shaped Particles (nano-tablet tube). Their composite shows a cauliflower shape. From the SEM images of Zeolite polypyrrole was encapsulating in the zeolite's materials.

The chemical composition or Elemental analysis for K, Al, Si, Ag, C, Cl, N and O in the pure Zeolite, modified Zeolite, Polypyrrole

and their composites were carried out using energy dispersive X-ray microanalysis. Samples for EDAX analysis were coated with thin gold foil in order to avoid charge influence. The corresponding electron dispersive spectra of these samples are shown in Figure 6 (a-d).

In the EDAX spectra, Zeolite-LTL sample was found to contain the elements like Potassium, Aluminium, Silicon and Oxygen; Modified Zeolite contain the elements like Potassium, Aluminium, Silicon, Oxygen and Silver; Polypyrrole

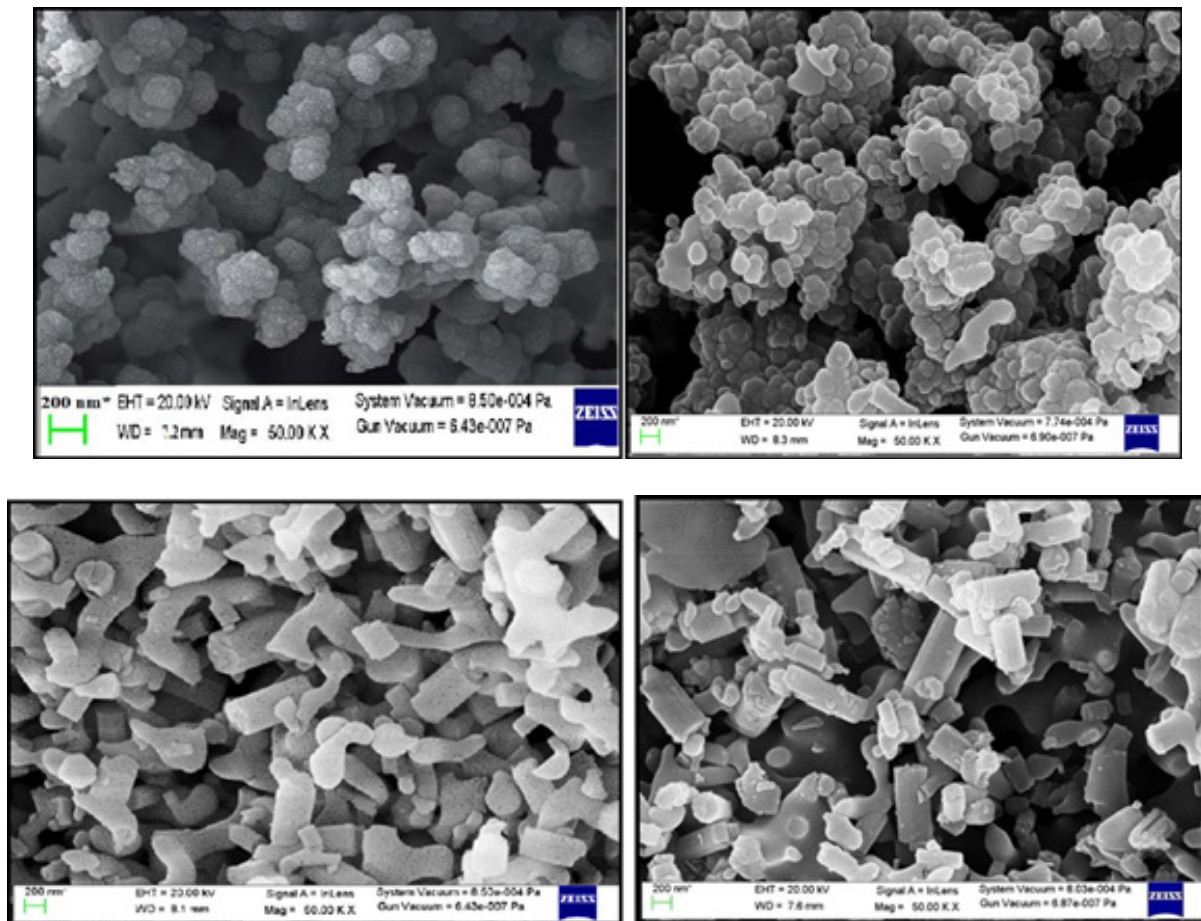


Figure 5. SEM Micrographs (a) Zeolite-LTL, (b) Ag-Zeolite-LTL, (c) PPy and (d) Composite.

particle contain the elements like Carbon, Oxygen, Sulfur and Nitrogen and these composites contain N, O, Al, Si, Cl, K, Ag and C elements indicating the successful of all the samples.

UV Vis Analysis

The optical properties of the Zeolite-Linde Type L and nano composite were determined by observing the optical absorption spectra. From the absorbance spectra, it is clearly

seen that both the sample shows optical activity in the visible region.

The direct energy gaps (band gap) were determined from the relation for direct band gap semiconductors by using the following equation:

$$(ah\nu)^2 = A (h\nu - E_g)$$

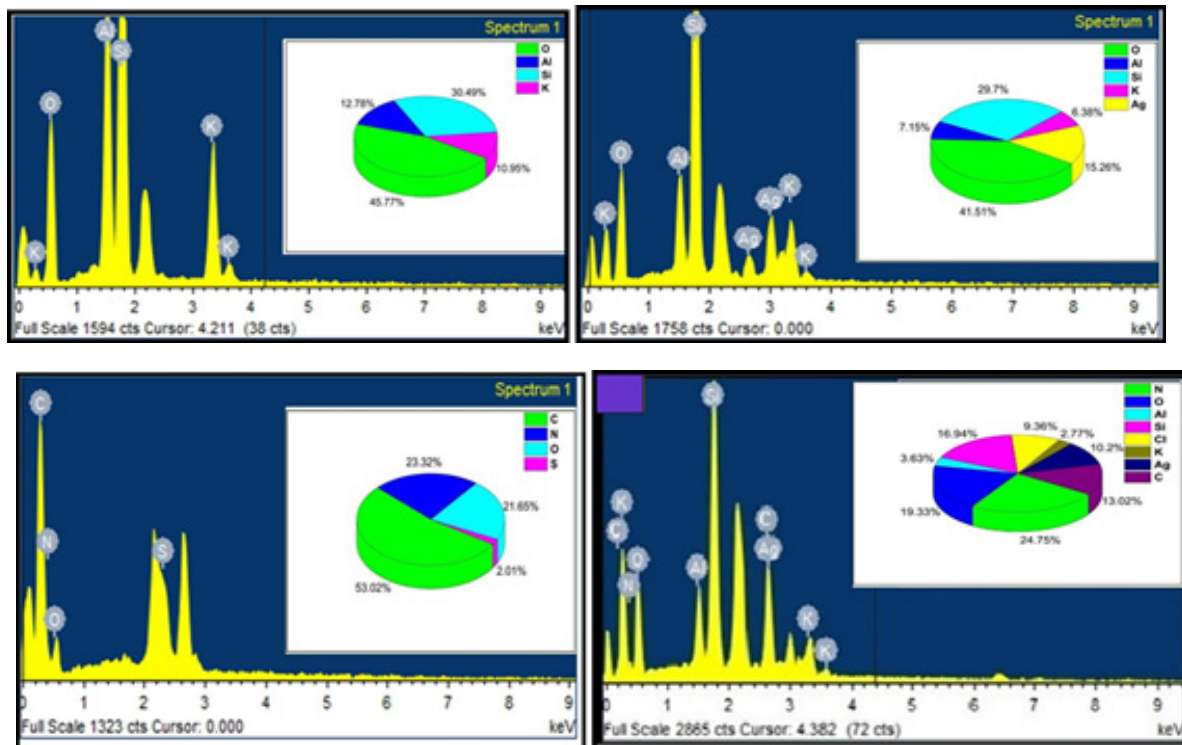


Figure 6. EDAX Spectrum of (a) Zeolite-LTL, (b) Ag-Zeolite-LTL, (c) PPy and (d) Composite.

$$\text{or, } (\alpha h\nu) = A (h\nu - E_g)^{1/2}$$

$$\text{or } \alpha h\nu = A (h\nu - E_g)^n$$

Where α - is the absorption coefficient and E_g - is optical energy band gap of the semiconducting material, A - is the proportionality constant and varies with the material, and n - represents the index.

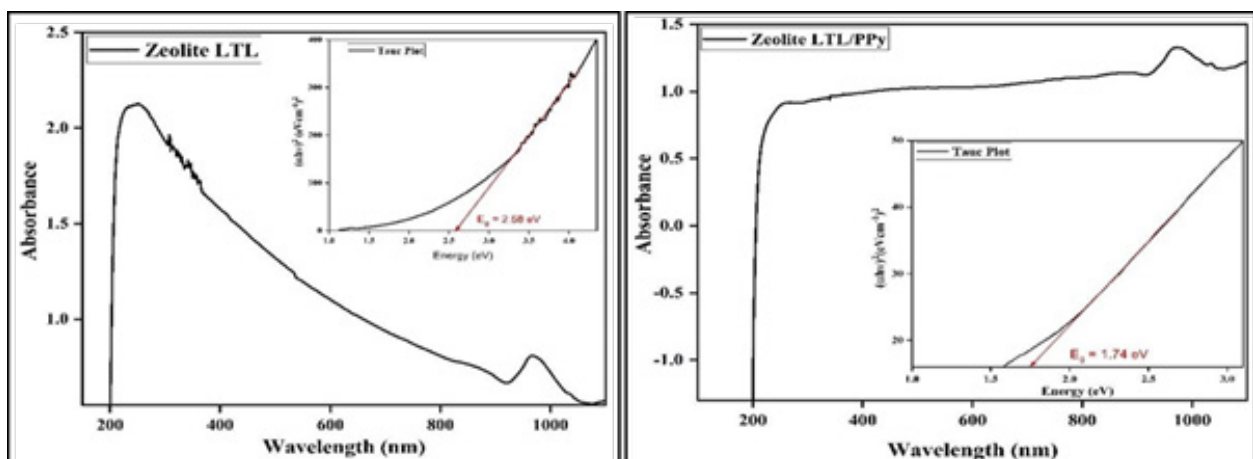


Figure 7. UV-Vis Spectra of synthesized (a) Zeolite-LTL (b) Composite.

The linear portion of the graphs drawn between $(ah\nu)^2$ and $h\nu$ was extrapolated, and the intercepts of these lines on the $h\nu$ axis correspond to the values of the optical energy gap (E_g) shown in figure 7 (a, b and c). The optical band gap of Zeolite-Linde Type L and its nano composite were found to be 2.58 and 1.74 eV, respectively.

Current density-voltage Characteristics

The DSSCs were characterized for photovoltaic performance under the light source of 100 W/cm^2 and the resulting in curves is shown in figure 8. The current-voltage (I-V) curve provides information regarding the operational parameters of the cell such as short-circuit current density (J_{sc}), open circuit voltage (V_{oc}), fill factor (FF), and overall conversion efficiency.

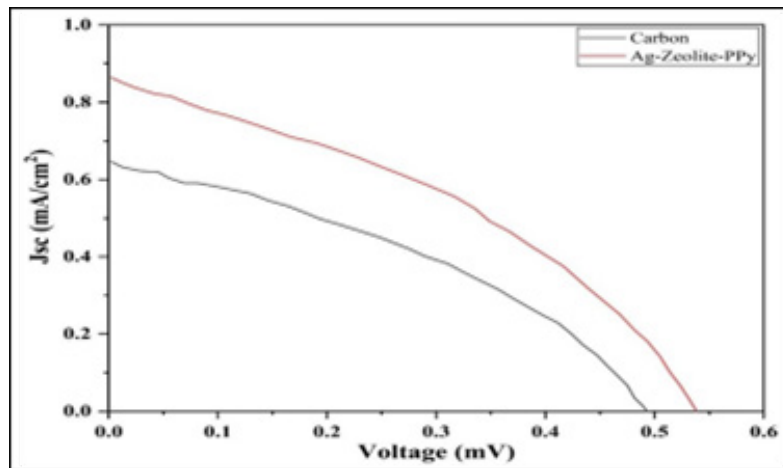


Figure 8. J-V characteristics of solar cell.

The FF and solar cell efficiency were obtained using equations 1 and 2 respectively;

$$FF = \frac{J_{max} \times V_{max}}{J_{sc} \times V_{oc}} \dots\dots(1)$$

$$\eta (\%) = \frac{J_{sc} \times V_{oc} \times FF}{I_{inc}} \times 100 \dots\dots(2)$$

Where V_{max} -maximum voltage; V_{oc} - open circuit voltage (Volt), J_{max} - Maximum current density; J_{sc} -short circuit current density (mA/cm^2) and I_{inc} -light intensity (W/cm^2).

The maximum power output, which is the ratio of output energy to the incident energy, was evaluated as follows;

$$P_{max} = J_{max} \times V_{max}$$

$$P_{max} = V_{max} \times I_{max}$$

The performance of solar cells can be seen through current measurements and voltage variations. The voltage measurement circuit in the solar cell construction is carried out using an unhindered circuit and with resistance (100 k Ω , 200 k Ω , 300 k Ω , 400 k Ω , 450 k Ω , 550 k Ω , and 620 k Ω) and a digital multimeter. Measurements are performed outdoors using sunlight as a light source. The resulting currents is calculated using Ohm's law approach, namely:

$$I = V/R$$

The point on the I-V curve yielding maximum current into voltage was called maximum power point (Max). The maximum power of solar cell was stated by,

Table 1. Efficiency Calculations of DSSC with different counter electrodes

Counter electrode	Jsc (mA/cm ²)	Voc (mV)	Fill Factor	Efficiency (%)
Carbon candle flame	0.39	0.293	0.46	0.143
Ag-Zeolite-PPy composite	0.57	0.300	0.57	0.214

CONCLUSION

In summary, the synthesis of Zeolite-Linde Type L and modified Zeolite was carried out by ion exchange method that is an environmentally friendly and synthesized by hydrothermal process and their composite was prepared by using the precipitation method. Structural properties determined were made by XRD and FTIR. The formation of the crystalline phase of the synthesized material is strongly supported by the XRD diffraction pattern. In addition, all samples are hexagonal phases, and the crystal size of the material is in the nanoscale. The SEM image shows the formation of a polyhedral structure of the Zeolite-Linde Type L, while the Zeolite Linde Type L/ PPy shows a cauliflower-like structure. The elemental composition of the synthesized material is in good agreement with the molecular formula of the synthesized material, as confirmed by EDAX analysis. The optical band gap of synthesis Linde Type L-Zeolite and its nanocomposite were found to be 2.58 and 1.74 eV, respectively. Finally, the photovoltaic efficiency of the Zeolite-Linde Type L/Polypyrrole nano composite shows a remarkable enhancement in the performance of N-719 dye under the illumination of light.

ACKNOWLEDGMENTS

The authors are very thankful to IIT Roorkee, for providing the SEM/EDAX facilities. We are also grateful to the CIF, Jiwaji University, Gwalior for extending the XRD, FTIR and optical facilities, respectively. We are also thank you to the department of physics and chemistry, jiwaji university, Gwalior for experiment support.

CONFLICT OF INTEREST

The authors declare that they have no known competing financial interests or personal relationships that could have appeared to influence the work reported in this paper.

DATA AVAILABILITY

All data related to the work is presented in this paper.

REFERENCES

- Kulprathipanja S. (Ed.). (2010). Zeolites in industrial separation and catalysis. United States: John Wiley & Sons.
- Faustini M, Nicole L, Ruiz-Hitzky E, Sanchez C. (2018). History of organic-inorganic hybrid materials: prehistory, art, science, and advanced applications. *Advanced Functional Materials*. 28(27):1704158.
- Kerstens D, Smeyers B, Van Waeyenberg J, Zhang Q, Yu J, Sels BF. (2020). State of the art and perspectives of hierarchical zeolites: practical overview of synthesis methods and use in catalysis. *Advanced Materials*. 32(44):2004690.
- Masoumifard N, Guillet-Nicolas R, Kleitz F. (2018). Synthesis of engineered zeolitic materials: from classical zeolites to hierarchical core-shell materials. *Advanced Materials*. 30(16):1704439.
- Beerdse E, Dubbeldam D, Smit B. (2006). Loading dependence of the diffusion coefficient of methane in nanoporous materials. *J Phys Chem B*. 110(45):22754-22772.
- Zhao C, Wu B, Tao Z, Li K, Li T, Gao X, Li Y. (2018). Synthesis of nano-sized LTL zeolite by addition of a Ba precursor with superior n-octane aromatization performance. *Catalysis Science & Technology*. 8(11):2860-2869.
- Hartmann M, Machoke AG, Schwieger W. (2016). Catalytic test reactions for the evaluation of hierarchical zeolites. *Chem Soc Rev*. 45(12):3313-3330.
- Zhao, C., Wu, B., Tao, Z., Li, K., Li, T., Gao, X., ... & Li, Y. (2018). Synthesis of nano-sized LTL zeolite by addition of a Ba precursor with superior n-octane aromatization performance. *Catalysis Science & Technology*, 8(11), 2860-2869.

9. Tahir MB, Kiran H, Iqbal T. (2019). The detoxification of heavy metals from aqueous environment using nano-photocatalysis approach: a review. *Environ Sci Pollut Res Int.* 26(11):10515-10528.
10. Assadullah I, Zaman MB, Malik KA, Malik JH, Bhat AA, Tomar R. (2021). Growth and properties of hydrothermally derived crystalline ZnSe quantum dots. *Environ Sci Pollut Res Int.* 28(4):3953-3959.
11. Bhat AA, Zaman MB, Malik JH, Malik KA, Assadullah I, Tomar R. (2021). Facile Way of Making Hydrothermally Synthesized Crystalline SrSnO₃ Perovskite Nanorods Suitable for Blue LEDs and Spintronic Applications. *ACS Omega.* 6(25):16356-16363.
12. Khaleque A, Alam MM, Hoque M, Mondal S, Haider JB, Xu B, et al. (2020). Zeolite synthesis from low-cost materials and environmental applications: a review. *Environmental Advances.* 2:100019.
13. Liu Y, Pang H, Wang X, Yu S, Chen Z, Zhang P, et al. (2021). Zeolitic imidazolate framework-based nanomaterials for the capture of heavy metal ions and radionuclides: a review. *Chemical Engineering Journal.* 406:127139.
14. Mallapur V P, Oubagaranadin JUK. (2017). A brief review on the synthesis of zeolites from hazardous wastes. *Transactions of the Indian Ceramic Society.* 76(1):1-13.
15. Koohsaryan E, Anbia M. (2016). Nanosized and hierarchical zeolites: A short review. *Chinese Journal of Catalysis.* 37(4):447-467.
16. Jongpatiwut S, Sackamduang P, Rirksomboon T, Osuwan S, Resasco DE. (2003). n-Octane aromatization on a Pt/KL catalyst prepared by vapor- phase impregnation. *Journal of catalysis.* 218(1):1-11.
17. Clark JH, Macquarrie DJ. (Eds.). (2008). *Handbook of green chemistry and technology.* United States: John Wiley & Sons.
18. Servatan M, Zarrintaj P, Mahmodi G, Kim SJ, Ganjali MR, Saeb MR, et al. (2020). Zeolites in drug delivery: Progress, challenges and opportunities. *Drug Discov Today.* 25(4):642-656.
19. Zhao C, Wu B, Tao Z, Li K, Li T, Gao X, et al. (2018). Synthesis of nano-sized LTL zeolite by addition of a Ba precursor with superior n-octane aromatization performance. *Catalysis Science & Technology.* 8(11):2860-2869.
20. Larlus O, Valtchev VP. (2004). Crystal morphology control of LTL-type zeolite crystals. *Chemistry of materials.* 16(17):3381-3389.
21. Tao Y, Kanoh H, Abrams L, Kaneko K. (2006). Mesopore-modified zeolites: preparation, characterization, and applications. *Chemical reviews.* 106(3):896-910.
22. Van Speybroeck V, Hemelsoet K, Joos L, Waroquier M, Bell RG, Catlow CR. (2015). Advances in theory and their application within the field of zeolite chemistry. *Chem Soc Rev.* 44(20):7044-7111.
23. Lupulescu AI, Kumar M, Rimer JD. (2013). A facile strategy to design zeolite L crystals with tunable morphology and surface architecture. *Journal of the American Chemical Society.* 135(17):6608-6617.
24. Zou X, Conradsson T, Klingstedt M, Dadachov MS, O'Keeffe M. (2005). A mesoporous germanium oxide with crystalline pore walls and its chiral derivative. *Nature.* 437(7059):716-719.
25. Li Y, Yu J. (2014). New stories of zeolite structures: their descriptions, determinations, predictions, and evaluations. *Chemical reviews.* 114(14):7268-7316.
26. Galstyan V, Comini E, Baratto C, Ponzoni A, Ferroni M, Poli N, et al. (2015). Large surface area biphasic titania for chemical sensing. *Sensors and Actuators B: Chemical.* 209:1091-1096.
27. Bhat AA, Assadullah I, Malik JH, Sharma A, Tomar R. (2021). Solvothermal synthesis of Fe doped MnSnO₃: An approach of wide bandgap perovskite towards optical, luminescence, and electrochemical properties. *International Journal of Energy Research.*
28. Bhat AA, Tomar R. (2021). Mn and Ce doping in hydrothermally derived CaSnO₃ perovskite nanostructure. A facile way to enhance optical, magnetic and electrochemical properties. *Journal of Alloys and Compounds.* 876:160043.

29. Gandla D, Sarkar S, Ghanti E, Ghosh S. (2017). Copper chromite- polyaniline nanocomposite: an advanced electrode material for high performance energy storage. *Electrochimica Acta*. 248:486-495.
30. Brunsteiner M, Jones AG, Pratola F, Price SL, Simons SJ. (2005). Toward a molecular understanding of crystal agglomeration. *Crystal Growth & Design*. 5(1):3-16.
31. Huo Y, Zhang J, Miao M, Jin Y. (2012). Solvothermal synthesis of flower- like BiOBr microspheres with highly visible-light photocatalytic performances. *Applied Catalysis B: Environmental*. 111:334-341.